New Rat Model that Phenotypically Resembles Autosomal Recessive Polycystic Kidney Disease

JEROEN NAUTA,* MIRIAM A. GOEDBLOED,* HARRY VAN HERCK,[§] DENNIS A. HESSELINK,* PIM VISSER,[‡] ROB WILLEMSEN,[‡] RICHARD P. E. VAN DOKKUM,[†] CHRISTOPHER J. WRIGHT,[‖] and LISA M. GUAY-WOODFORD[‖¶#]

*Departments of *Pediatrics, [†]Pediatric Surgery, and [‡]Cell Biology, Erasmus Medical Center Rotterdam, Rotterdam, The Netherlands; [§]Central Laboratory Animal Institute, Utrecht University, Utrecht, The Netherlands; and Departments of [‖]Cell Biology, [¶]Pediatrics, and [#]Medicine, University of Alabama at Birmingham, Birmingham, Alabama.*

Abstract. Numerous murine models of polycystic kidney disease (PKD) have been described. While mouse models are particularly well suited for investigating the molecular pathogenesis of PKD, rats are well established as an experimental model of renal physiologic processes. Han:SPRD-*Cy* rats have been proposed as a model for human autosomal dominant PKD. A new spontaneous rat mutation, designated *wpk*, has now been identified. In the mutants, the renal cystic phenotype resembles human autosomal recessive PKD (ARPKD). This study was designed to characterize the clinical and histopathologic features of *wpk/wpk* mutants and to map the *wpk* locus. Homozygous mutants developed nephromegaly, hypertension, proteinuria, impaired urine-concentrating capacity, and uremia, resulting in death at 4 wk of age. Early cysts were present in the nephrogenic zone at embryonic day 19. These were localized, by specific staining and electron microscopy, to differentiated proximal tubules, thick limbs, distal tubules, and collecting ducts. In later stages, the cysts were largely confined to collecting ducts. Although the renal histopathologic features are strikingly similar to those of human ARPKD, *wpk/wpk* mutants exhibited no evidence of biliary tract abnormalities. The *wpk* locus maps just proximal to the *Cy* locus on rat chromosome 5, and complementation studies demonstrated that these loci are not allelic. It is concluded that the clinical and renal histopathologic features of this new rat model strongly resemble those of human ARPKD. Although homology mapping indicates that rat *wpk* and human ARPKD involve distinct genes, this new rat mutation provides an excellent experimental model to study the molecular pathogenesis and renal pathophysiologic features of recessive PKD.

Renal cystogenesis occurs with a number of inherited, developmental, and acquired diseases (1). A common feature among this otherwise heterogeneous set of disorders is the development of epithelium-lined cysts arising from various nephron segments and the collecting ducts.

Of these conditions, the inherited polycystic kidney diseases (PKD) have been most extensively investigated. These disorders, which are transmitted as single Mendelian traits, cause significant morbidity and death among both adults and children (2). Autosomal dominant PKD (ADPKD) causes 6 to 8% of end-stage renal disease among adult patients. With autosomal recessive PKD (ARPKD), 30 to 50% of affected neonates die in the perinatal period. Surviving ARPKD patients, in combination with children with juvenile nephronophthisis, comprise 6 to 14% of all pediatric patients with end-stage renal disease (3,4).

Received November 16, 1999. Accepted May 15, 2000.
Correspondence to Dr. J. Nauta, Sophia Childrens Hospital, Molewaterplein 60, 3015 GJ Rotterdam, The Netherlands. Phone: 31-10-4636363; Fax: 31-10-4636801; E-mail: nauta@alkg.azr.nl

1046-6673/1112-2272
Journal of the American Society of Nephrology

Recent genetic studies have identified the principal genes involved in ADPKD (*PKD1* and *PKD2*) (5,6). In addition, linkage studies have defined the predominant, if not exclusive, locus for ARPKD (*PKHD1*) (7,8). Although ADPKD is inherited as a dominant trait, multiple lines of evidence indicate that a second somatic mutation in this disorder may be necessary for disease expression (9,10). This suggests that, like ARPKD, ADPKD is initiated by recessive cellular mechanisms. However, the molecular pathogenic events involved in the initiation and progression of renal cystic diseases remain largely unknown.

In addition to human PKD, numerous mouse and rat models have been described (11–13). Most of these involve disruption of a single gene, and the mutant phenotypes closely resemble human PKD with respect to morphologic features, cyst localization, and disease progression. Several models are the result of spontaneous mutations, whereas others were engineered through either chemical mutagenesis or transgenic technologies. In addition, experimental models of PKD have been induced by chemical cystogens, primarily in rats.

Although the numerous mouse PKD mutations provide powerful models to characterize the genetic factors that regulate renal cyst initiation and disease progression, these models have limited utility for renal physiologic investigations. In contrast,

rats represent a well established model system for investigating renal physiologic parameters such as renal blood flow, GFR, renal tubular transport, and BP regulation. In rats, PKD has been reported in the Han:SPRD-*Cy* model (14) and the Wistar-*chi* model (15). Han:SPRD-*Cy* rats have been well characterized and have been studied extensively as a model of ADPKD. The renal cystic disease in the Wistar-*chi* model resembles ARPKD in that lectin-binding studies localize the tubular cysts to collecting ducts. However, unlike in human ARPKD, the renal insufficiency progresses slowly and is associated with skeletal abnormalities.

In this report, we describe a new rat PKD model. Affected homozygotes develop rapidly progressive PKD that clinically and histologically resembles human ARPKD. This mutation occurred spontaneously in an outbred Wistar strain. We therefore designated the mutant locus *wpk* (Wistar polycystic kidneys). We have localized *wpk* to chromosome 5. This locus is distinct from the rat Han:SPRD-*Cy* locus, and its mouse and human orthologs are not allelic with any previously described mouse PKD model or human PKD gene. However, on the basis of the phenotypic similarities with human ARPKD, *wpk* rats provide a new experimental model for investigating the pathogenesis of recessive PKD. Because renal physiologic features have been well studied in rats, *wpk* rats should provide the first model system for evaluation of the abnormalities in renal tubular transport and systemic BP regulation that are associated with recessive PKD.

Materials and Methods

Rats

The *wpk* mutation was first recognized in 1994 in a colony of outbred Wistar rats, U:WU (Cpb), at Utrecht University (Utrecht, The Netherlands). This breeding colony was initiated in 1989 from 10 ancestral breeding pairs obtained from the National Institute of Public Health and the Environment (RIVM; Bilthoven, The Netherlands). No new rats have been introduced into the colony since 1989. In 1996, a breeding pair of test-proven heterozygotes were transferred to the University of Rotterdam (Rotterdam, The Netherlands), and a new subcolony was initiated. This colony has been maintained by brother-sister matings for more than five generations. Individuals heterozygous for the mutant allele were identified in each generation by test-crossing phenotypically normal offspring from known heterozygotes.

The Han:SPRD-*Cy* rat model of PKD (16) was used in complementation experiments and as a phenotypic reference for our evaluation of the homozygous *wpk/wpk* rats. In this model, *+/Cy* heterozygotes develop slowly progressive PKD that leads to renal failure in male animals only, at ≥6 mo of age, whereas *Cy/Cy* homozygotes develop a severe form of PKD within the first few weeks of life. Heterozygous Han:SPRD-*+/Cy* breeding pairs were kindly provided in 1994 by F. Deerberg (Central Institute for Laboratory Animal Breeding, Hannover, Germany), and a breeding colony was established at the University of Rotterdam. BB-DP rats, an inbred strain (F30) derived from biobreeding, diabetes mellitus-prone rats, were kindly provided by H. A. Drexhage (Department of Immunology, Erasmus University, Rotterdam, The Netherlands).

To map the *wpk* locus, we used a (Wistar-*+/wpk* × BB-DP)F1 intercross, which was initially generated to test linkage to the *PKD1* locus. The inbred BB-DP strain was selected on the basis of its genotype of *Prm1*, a polymorphic marker that is tightly linked to the rat *PKD1* locus (17). Wistar-*+/wpk* heterozygotes of both genders were bred with BB-DP rats, and F1 progeny heterozygous for the *wpk* mutation were intercrossed to generate F2 rats. Affected homozygotes could be identified by abdominal palpation on postnatal day 12.

All animals were fed standard rat chow containing 24% protein and had free access to acidified tap water (pH 2.5 to 3.0). All experiments were conducted in accordance with the Dutch guidelines for the care and use of laboratory animals.

Clinical Parameters

Kidney weight, body weight, BP, and urine and blood chemistry values were assessed for groups of six to eight rats at the age of 3 to 4 wk. Affected *wpk/wpk* rats were compared with phenotypically unaffected littermates. Affected *Cy/Cy* rats were compared with +/+ littermates. In contrast to *+/wpk* heterozygotes, *+/Cy* rats could be identified histologically, and these pups were excluded from further analysis.

The weights of the left and right kidneys of *wpk/wpk* homozygotes did not differ. The kidney weights were therefore combined and expressed as a percentage of body weight. Data for male and female pups were pooled, because gender effects were never observed for prepubertal animals.

BP was measured in six pairs of 3- to 4-wk-old rats anesthetized with ketamine and thiopental, using an indwelling catheter in the femoral artery. Blood was obtained, by cardiac puncture, from six pairs of *wpk/wpk* homozygotes and unaffected littermates. Urea nitrogen, creatinine, and total bilirubin levels were measured in the plasma using a Kodak Ektachem 700 spectrophotometer (Kodak, Utrecht, The Netherlands). Urine was collected after cervical dislocation, after 2 h of fasting, from 4-wk-old affected and unaffected *wpk* rats. Urinary creatinine levels were measured by the Jaffé method and urinary protein levels by absorption spectroscopy.

For older animals, urinary protein excretion, BP, and blood chemistry values were compared between test-proven heterozygous *+/wpk* rats and wild-type control animals, at the age of 1.5 yr for female animals and 1 yr for male animals. Twenty-four-hour urine specimens were collected using metabolic cages. BP was determined by tail plethysmography. The animals were trained for this procedure before the measurements (18). Blood was obtained by aortic puncture, with ether anesthesia.

Tissue Preparation for Histologic Analysis and Electron Microscopy (EM)

For histologic analysis, kidneys were obtained from *wpk/wpk* and control animals on embryonic day 19 and postnatal days 0, 7, 14, and 21. The cystic phenotype was established by histologic assessment. Multiple-organ necropsies, including heart, lung, liver, pancreas, spleen, brain, and intestine, were performed on 21-d-old homozygous mutants and adult heterozygotes. Heterozygous female animals were studied at the age of 1.5 yr and male animals were studied at the age of 1 yr.

For light microscopic and immunohistochemical analyses, the kidneys and livers were fixed in 4% paraformaldehyde in phosphate-buffered saline (PBS) (pH 7.4) and embedded in paraffin. For liver histologic analyses, the left ventral lobe was dissected, fixed in 4% paraformaldehyde in PBS, and embedded in paraffin with the convexity toward the surface of the block.

For EM, representative kidney samples were fixed in 2.5% glutaraldehyde, postfixed in 1% osmium tetroxide, and dehydrated in a graded alcohol series. For scanning EM, the samples were then critical

point-dried, mounted on stubs, coated with gold/palladium, and examined with a JEOL JSM 25 scanning electron microscope (JEOL, Tokyo, Japan). For transmission EM, the fixed and dehydrated samples were embedded in Epon. Thin sections were stained with uranyl acetate and lead citrate and examined with a Philips C100 electron microscope (Philips, Eindhoven, The Netherlands). Human kidney tissue from a neonate with ARPKD and end-stage renal failure was used as a comparative reference for the scanning EM analyses of *wpk/wpk* kidneys.

Evaluation of Biliary Ductal Plates

In addition to the renal cystic lesions, intrahepatic morphologic features were evaluated for six affected *wpk/wpk* homozygotes and six phenotypically unaffected animals (age, 21 d). The depth and angle of the liver sections were standardized for histologic and morphometric analyses, as described previously (19). Bile ductules and recognizable portal areas were systematically examined in each section, by one observer blinded to the phenotypes of the animals. A recognizable portal area was defined as a venule accompanied by one or more bile ductules.

Immunohistochemical Analyses

The localization of the renal cysts was evaluated by immunodetection of nephron segment-specific proteins and lectin binding sites, on postnatal days 0, 7, 14, and 21. On the basis of preliminary studies, the following reagents were selected. As a rat proximal tubule marker, we used polyclonal goat anti-rat dipeptidyl peptidase 4 (dpp4) at dilutions of 1:500 (kindly provided by E. de Heer, Leiden University Medical Center, Leiden, The Netherlands) (20). As a marker of the thin limb of Henle's loop (medulla) and proximal tubules (cortex), we used polyclonal rabbit anti-rat aquaporin-1 (Aqp1) at 1:100 (generous gift of P. Deen, University of Nijmegen, Nijmegen, The Netherlands). As a marker of the thick ascending limb, we used polyclonal rabbit anti-human Tamm-Horsfall glycoprotein at 1:200 (Biomedical Technologies, Stoughton, MA). As a marker of cortical and medullary collecting tubules, we used polyclonal rabbit anti-rat Aqp2 at 1:100 (generous gift of P. Deen, University of Nijmegen). All antibodies were diluted in PBS with 0.5% dried milk and 0.15% glycine.

Schäfer *et al.* (16) reported increased expression of collagen type IV and laminin in the renal cysts of 2-mo-old Han:SPRD-+/*Cy* rats. Therefore, for comparative purposes, kidney sections from 21-d-old Wistar-*wpk/wpk* rats, 21-d-old Han:SPRD-*Cy/Cy* rats, and 2-mo-old +/*Cy* rats were analyzed with Jones' silver stain, as well as with a polyclonal rabbit anti-mouse collagen IV antibody at 1:200 (Collaborative Medical Products) (21) and a polyclonal rabbit anti-mouse laminin antibody at 1:50 (Eurodiagnostica, Arnhem, The Netherlands) (22).

The tissue sections were pretreated with 0.1% pronase in PBS for 5 to 10 min before the incubations with anti-Tamm-Horsfall glycoprotein, anti-dpp4, and anti-collagen IV and with 0.2% sodium dodecyl sulfate in PBS for 5 min before the incubations with anti-Aqp2. Anti-laminin and anti-Aqp1 were used without pretreatment of the tissue sections. Primary rabbit antibodies were detected using swine anti-rabbit peroxidase conjugate at 1:100 (Dako). Goat anti-dpp4 was detected using rabbit anti-goat peroxidase conjugate at 1:100 (Dako). The sections were stained with 0.05% diaminobenzidine/0.01% hydrogen peroxide and counterstained with hematoxylin.

Statistical Analyses

Clinical data are expressed as means and SD. Differences between *wpk* and control animals were analyzed by *t* test.

PCR-Based Genotyping

To type progeny for the inheritance of alleles of anonymous DNA microsatellite markers, spleen genomic DNA was prepared according to standard protocols. Initial mapping was performed using interval haplotype analysis (23). For these studies, we selected microsatellite markers whose Wistar and BB-DP alleles differed in size by at least 6 bp and mapped within approximately 10 cM of the proximal and distal ends of each chromosome.

After chromosomal localization, further mapping was performed using markers spaced at 20-cM intervals along chromosome 5 (low-resolution linkage mapping study) and then within 4 cM of *D5Rat73* (high-resolution linkage mapping study). All markers were chosen from the on-line Whitehead/Massachusetts of Technology database [accessible at http://www-genome.wi.mit.edu/; described by Szpirer *et al.* (24)]. PCR primer pairs for these markers were purchased from Research Genetics (Huntsville, AL).

Forward primers were end-labeled with [γ-^{32}P]ATP, and PCR amplification was performed as described (25). Amplified fragments were analyzed on denaturing 6% polyacrylamide gels.

Analysis of Genetic Data

Genotype data, obtained by analyzing 35 affected F2 progeny for microsatellite markers known to map to the ends of each autosome, were subjected to interval haplotype analysis exactly as described by Neuhaus and Beier (23). To construct low- and high-resolution linkage maps, individual chromosomal haplotypes were inferred from F2 genotypic data, as described previously (25), and markers were ordered to minimize the numbers of crossover events needed to account for the inferred haplotypes.

Results

Wistar-wpk/wpk Phenotype

Our Wistar-+/*wpk* colony breeding has been maintained for more than five generations, using a system of brother-sister matings. Heterozygotes exhibited a normal phenotype and bred as productively as wild-type Wistar rats. A typical litter contained 9 to 14 pups. As expected for an autosomal trait, approximately one-fourth of the offspring of test-proven heterozygotes expressed PKD, and male and female animals were affected in equal numbers (23.5 and 24.2%, respectively). Of note, approximately 10% of the F1 pups died within the first 2 wk of postnatal life. These were not available for systematic studies, because dead pups are generally eaten by the parents.

The phenotype of homozygous mutants was characterized by progressive nephromegaly and abdominal distension. Nephromegaly was first palpable on postnatal day 12. By 4 wk of age, homozygous mutants were runted and had large palpable kidneys. Affected rats died at 4 to 6 wk of age. The total kidney weight was $\geq$10% of the body weight at 4 wk (Table 1). In comparison, the kidney weight was 1% of the body weight for unaffected littermates and 20% of the body weight for Han:SPRD-*Cy/Cy* mutants at the same age. At 3 wk of age, *wpk/wpk* homozygotes exhibited elevated plasma urea and creatinine levels, proteinuria, and low urine osmolality after 2 h of fasting, compared with unaffected littermates. The mean arterial BP, as assessed under anesthesia by direct measurement in the femoral artery, was markedly elevated (Table 1). The weight of the liver relative to the kidney-free body weight

Table 1. Clinical features of homozygous mutants and unaffected littermates at 3 to 4 wk of age[a]

	Wistar		Han:SPRD-*Cy*	
	wpk/wpk	Unaffected	*Cy/Cy*	+/+
Body weight (g)	43.3 ± 6.8	48.2 ± 7.2	34.3 ± 3.5	38.1 ± 5.8
Kidney weight/body weight × 100 (%)	10.9 ± 0.6[b]	1.1 ± 0.1	21.8 ± 1.4[b]	1.0 ± 0.5
BP (mmHg) (mean)	139 ± 26[b]	90 ± 10	ND	ND
Plasma urea concentration (mM)	29.3 ± 2.8[b]	8.9 ± 0.7	51.2 ± 8.8[b]	13.2 ± 1.7
Plasma creatinine concentration (μM)	42 ± 11[b]	24 ± 9	70 ± 15[b]	35 ± 10
Urinary protein excretion (mg/mmol of creatinine)	580 ± 307[b]	33 ± 26	ND	ND
Urine osmolality (mosmol/kg)	394 ± 87[b]	961 ± 584	ND	ND

[a] Body weight, kidney weight, and plasma concentrations of urea and creatinine were measured for 3-wk-old rats; proteinuria, urine osmolality, and mean BP were measured for 3- to 4-wk-old rats. Values are given as means ± SD. ND, not done.
[b] $P < 0.01$ *versus* controls.

and the plasma bilirubin levels were not significantly different for homozygous mutants *versus* unaffected littermates.

Test-proven heterozygotes were clinically unaffected. There was no significant difference between 18-mo-old female +/*wpk* heterozygotes and age-matched, wild-type, control animals with respect to body weight (345 ± 24 *versus* 344 ± 29 g), systolic BP (135 ± 9 *versus* 128 ± 7 mmHg), plasma creatinine levels (41 ± 4 *versus* 46 ± 5 μM), or urinary protein excretion rate (20 ± 13 *versus* 27 ± 18 mg/d per 100 g body wt). Similarly, 1-yr-old male +/*wpk* heterozygotes did not differ from age-matched control animals with respect to body weight (547 ± 31 *versus* 517 ± 25 g), systolic BP (130 ± 7 *versus* 127 ± 8 mmHg), plasma creatinine levels (47 ± 5 *versus* 49 ± 7 μM), or urinary protein excretion rate (40 ± 26 *versus* 38 ± 21 mg/d per 100 g body wt).

Pathologic Features of wpk/wpk Kidneys

At a gross level, neonatal *wpk/wpk* kidneys exhibited normal architecture, including normal lobulation, medullary rays, and well defined corticomedullary demarcation. In affected pups, the kidneys progressively enlarged but maintained a reniform shape, despite the progressive cystic changes in the parenchyma. The capsular surface was smooth. The renal pelvis and calices were not enlarged and maintained a normal relation to the parenchyma (Figure 1). The ureters were present and nondilated. This pattern is very similar to that observed in the kidneys of human neonates with ARPKD.

The histopathologic findings were characterized by progressive cystic dilation of the renal tubules. Early cysts were noted at 19 d of embryonic development (Figure 2, A and B). At that stage, as well as in neonatal kidneys, the lesions were predominantly localized in the renal cortex. The cysts were round or oval and were lined with either a single layer of cuboidal cells or flattened epithelia (Figure 2C). Some of the cysts were lined by a brush border-bearing cell type, suggesting proximal tubular epithelia. The cell density of the epithelial lining was high in most but not all cysts. Glomerular cysts were not observed.

With subsequent disease progression, cysts developed throughout the entire kidney (Figure 2D); cortical cysts were arrayed in a radial orientation, whereas medullary cysts were generally round and of variable size. In kidneys with advanced

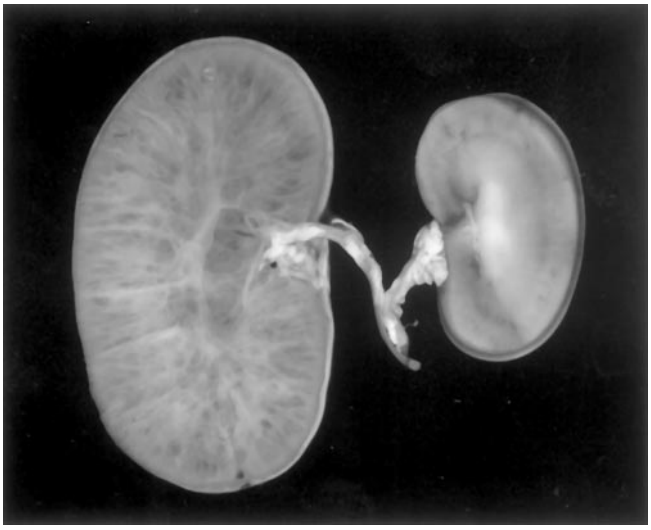

Figure 1. Normal (right) and cystic (left) kidneys at 3 wk of age. Magnification, ×2.3. The affected kidney has a well maintained reniform shape, a smooth capsular surface, and radially oriented cysts. The renal pelvis and ureters are not dilated.

cystic disease, there was an apparent reduction in the number of glomeruli and nondilated tubules, and those remaining appeared to be compressed between innumerable tubular cysts. Interstitial fibrosis was not observed, and the renal vasculature was unremarkable. In contrast to the early cystic kidneys, the cysts in more advanced disease were lined with a relatively homogeneous cell type. Within individual cysts, the cell densities varied considerably. Interestingly, areas of high cell density were often juxtaposed with similar areas in neighboring cysts (Figure 2E). This observation suggests that focal epithelial cell proliferation within cysts may be determined by the local biologic environment. However, true epithelial hyperplasia with associated polyps or microadenomas, as noted in human ADPKD (26), in *Cy/Cy* rats (16), and in the c-*myc*-overexpression model of PKD (27), was never observed.

Immunohistochemical Analyses

Cysts in neonatal kidneys were stained with either anti-dpp4, anti-Tamm-Horsfall protein, or (from day 1 onward) anti-Aqp2

antibody, indicating cellular characteristics typical of proximal tubules, thick ascending limbs, or collecting tubules, respectively. Staining of medullary cysts with anti-Aqp1, indicating a thin loop-derived cell type, was rarely observed. Cortical cysts were occasionally stained with anti-Aqp1 in a weak pattern. These cysts were lined by a brush border-bearing cell type and were also stained with anti-dpp4, indicating proximal tubules. Individual cysts were typically lined with only one cell type, and overlapping staining patterns (except for anti-Aqp1 staining in proximal tubules) were not observed. By 2 wk of age, the vast majority of cysts appeared to be derived from collecting ducts, because the majority of cysts were stained with anti-Aqp2. At 3 wk of age, >90% of the cysts expressed Aqp2 (Figure 2F). In comparison, renal cysts in 3-wk-old *Cy/Cy* homozygotes appeared to arise from all nephron segments (data not shown).

In *wpk/wpk* homozygotes, the renal tubular basement membrane morphologic features, as assessed with Jones' silver staining, were not significantly different between cystic tubules and normal tubules in either early or advanced disease. Moreover, there was no difference in the expression of the tubular basement membrane constituents collagen type IV and laminin when cystic and noncystic tubules were compared. In contrast, collagen type IV and laminin were overexpressed in the tubular basement membranes associated with some but not all renal tubular cysts in SRPD-+/*Cy* and SRPD-*Cy/Cy* kidneys (data not shown) (16).

Electron Microscopy

Scanning EM results were consistent with the light microscopic observation that early and late cysts have different epithelial linings (Figure 3). The cell surface characteristics of early cystic tubules varied considerably among individual cysts. Some tubules exhibited a homogeneous brush border,

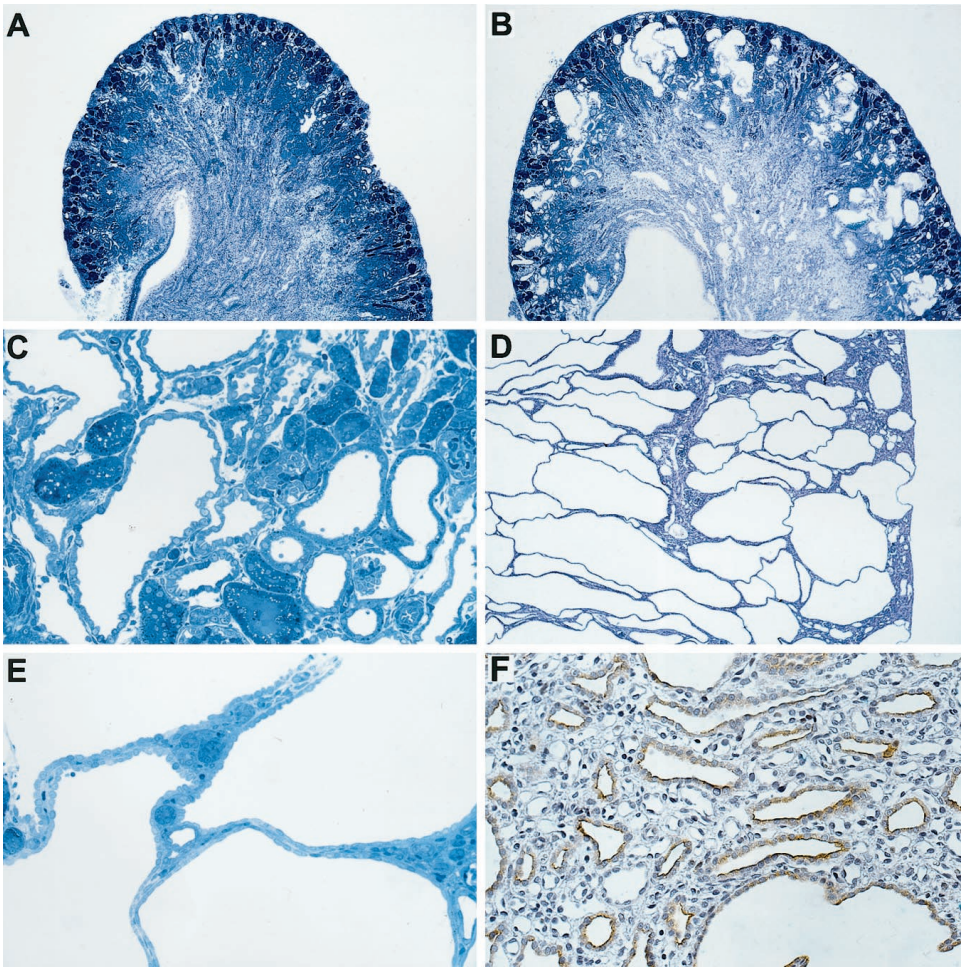

Figure 2. Light microscopy of kidneys at different ages. (A and B) Normal (A) and cystic (B) kidneys at embryonic day 19. Clusters of cysts in the cortex suggest that adjacent cysts are dilations of tubular loops of the same nephron. Medullary cysts are markedly smaller. Hematoxylin; magnification, ×30. (C) Neonatal kidney with cortical cysts lined by various types of epithelium. Methylene blue; magnification, ×120. (D) Cortical area of an end-stage cystic kidney, exhibiting large epithelial cysts. Glomerular cysts were not observed. The few glomeruli and nondilated tubules seem to be compressed between innumerable cysts. Hematoxylin; magnification, ×30. (E) Considerable variation in cell densities within individual cysts. Areas of high cell density were often juxtaposed with similar areas in neighboring cysts. Methylene blue; magnification, ×80. (F) Aquaporin-2 (Aqp2) staining of the vast majority of cysts in a 3-wk-old cystic kidney. Diaminobenzidine and hematoxylin; magnification, ×100.

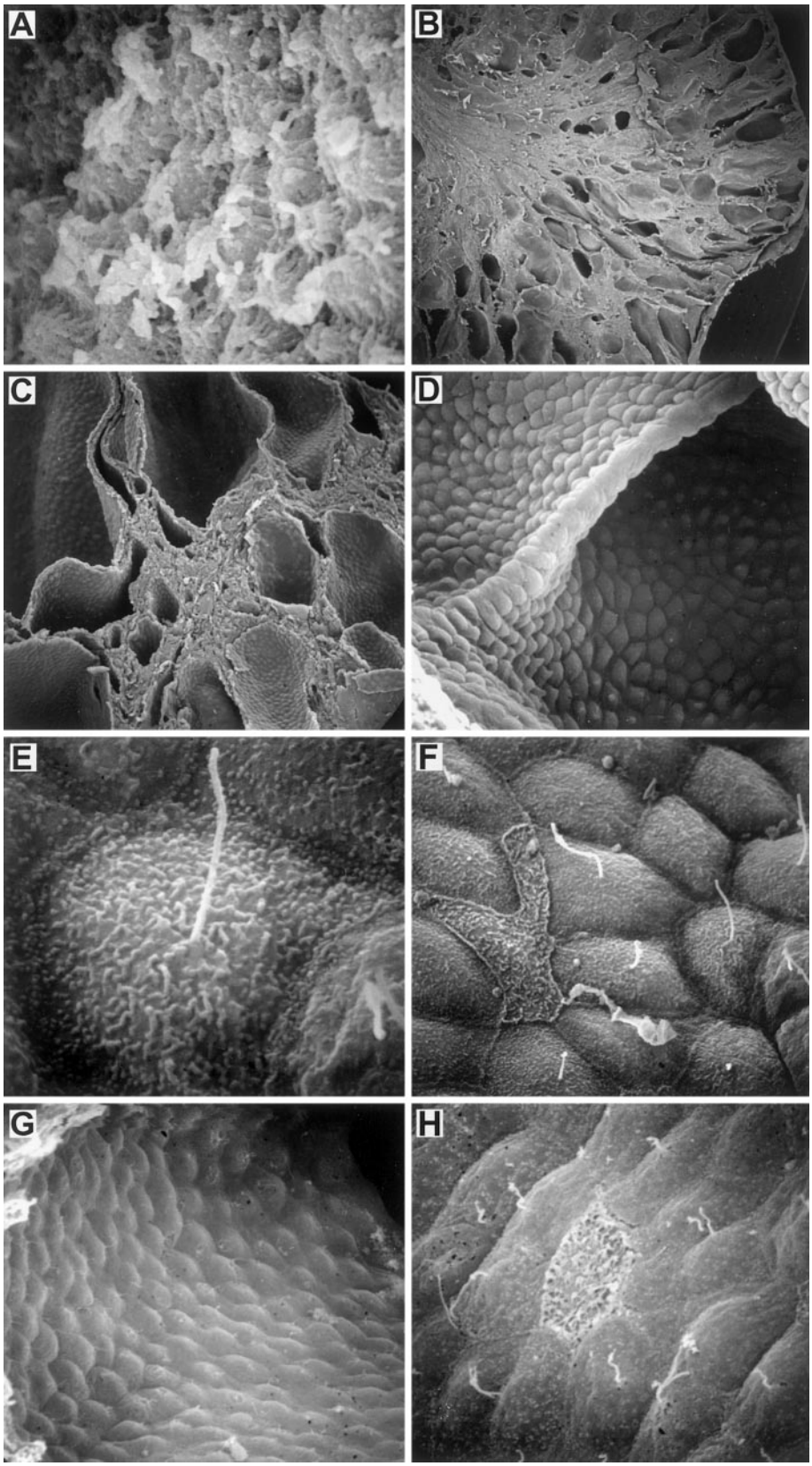

Figure 3. Scanning electron microscopy (EM) of renal cysts in neonatal (A) and 3-wk-old (B to F) affected *wpk/wpk* rats and of an end-stage human autosomal recessive polycystic kidney disease (ARPKD) kidney (G and H). (A) A neonatal *wpk/wpk* cyst is lined by a brush border-bearing cell type, suggesting a proximal tubular cell type. (B) In this 3-wk-old *wpk/wpk* kidney, radially aligned fusiform cysts can be observed, at low magnification, in the cortex, with more rounded cysts in the medulla. (C) At this stage, the cysts are densely packed and the epithelia of adjacent cysts are often juxtaposed, with little interstitial tissue between them. Normal renal structures can barely be identified. (D)

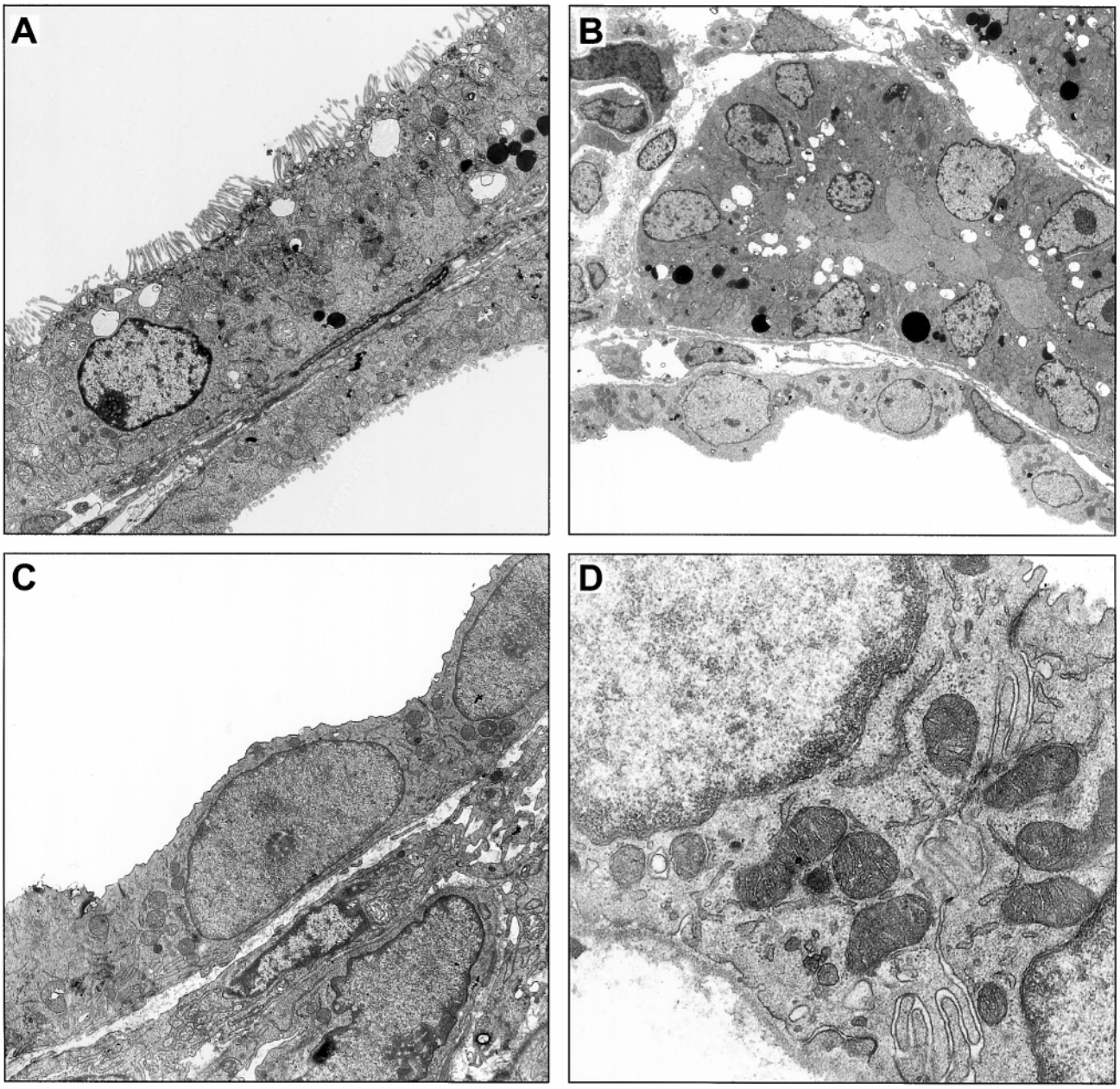

Figure 4. Transmission EM of renal lesions in neonatal (A and B) and 3-wk-old (C and D) *wpk/wpk* rats. (A) Neonatal cyst lined by proximal tubular epithelium. The cells are characterized by a well differentiated brush border, an apical endosomal/lysosomal apparatus, a dense network of microtubules, normal intracellular organelles (including peroxisomes), and many mitochondria, which are short and randomly distributed. The basal laminae are regular and intact. Magnification, ×4000. (B) Cortical cyst lined by collecting tubular cells, featuring a relatively smooth cell surface, apical tubulovesicular profiles, and a regular basement membrane of normal thickness. Magnification, ×3000. (C) Cyst-lining cells of a 3-wk-old affected rat. The characteristics of principle cells include a fairly smooth apical surface, a few short microvilli, basolateral folds, a tight cytoplasmic network of tubulovesicular profiles below the apical membrane, and sparse mitochondria. The basal laminae are intact and regular. Magnification, ×5000. (D) Evidence that the intercellular junctions of these cells are relatively deep and tight and the cells have narrow folds of cytoplasm that interlock with counterparts of adjacent cells. Magnification, ×25,000.

Figure 3 (*Continued*). The vast majority of cysts are lined by a homogeneous cobblestone-like cell pattern. (E) Most cells have the typical characteristics of principle cells, including a relatively smooth rounded surface and a single cilium. (F) Other cells have the characteristics of intercalated cells, including a relatively rough angular surface and no cilium. The microprojections are moderate in both size and number, as described for type B intercalated cells (28). (G and H) Human ARPKD cysts are typically lined with a homogeneous cobblestone-like cell pattern (G) and a mixture of principle and intercalated cells (H). Magnification: ×6500 in A; ×10 in B; ×100 in C; ×450 in D; ×6500 in E; ×2000 in F; ×650 in G; ×2000 in H.

characteristic of proximal tubules (Figure 3A). Others exhibited more distal tubule or collecting duct characteristics, including fewer microvilli and smoother apical surfaces. Some exhibited the typical characteristics of collecting ducts, with a prominent single cilium, as illustrated for 3-wk-old tissue (Figure 3E).

Cysts in kidneys with advanced disease were radially oriented. In contrast to early cysts, these cysts were uniformly lined by a homogeneous cobblestone cell type, indicating a collecting duct origin (Figure 3, B to D). These cells exhibited the typical phenotype of principal cells, including relatively smooth apical surfaces and a well differentiated, conspicuous, single cilium (Figure 3E). These cilia were prominent for the vast majority of cortical cysts and less prominent or absent for medullary cysts. In addition, the epithelial lining of most cysts contained a small number of rough-surfaced cells with characteristics previously described for rat type B intercalated cells (Figure 3F) (28). This mixed pattern of principal and intercalated cells is characteristic of cortical and outer medullary collecting ducts in rats and is very similar to the pattern observed for the vast majority of the cysts in our human ARPKD reference sample (Figure 3, G and H) (28).

Transmission EM results were consistent with both the light microscopic and scanning EM findings. Early renal cysts in *wpk/wpk* rats were lined by well differentiated cells with the phenotypic characteristics of either proximal tubules, thick ascending limbs, distal tubules, or collecting ducts (Figure 4). Microvilli were well formed, cell junctions and basal laminae were intact, and the cellular organelles were normally distributed. At 3 wk of age, the vast majority of cortical and medullary cysts were lined by a homogeneous layer of cells with the characteristic phenotype of collecting duct cells (29). Abnormalities evident in human ADPKD and in the Han:SPRD-*Cy/Cy* model, *e.g.*, basement membrane thickening, intercellular vacuoles, or intratubular micropolyps, were not observed (26). The basal laminae were intact, with normal architecture and thickness.

Nonrenal Tissues

Multiorgan necropsies of 3-wk-old Wistar-*wpk/wpk* pups and adult Wistar-+/*wpk* heterozygotes did not reveal any nonrenal structural abnormalities. Of particular note, no evidence of ductal plate malformations or biliary cysts was observed by light microscopy in multiple liver sections from six 3-wk-old *wpk/wpk* rats. Morphometric analyses of standardized liver sections revealed no evidence of portal triad abnormalities or bile ductule proliferation in *wpk/wpk* homozygotes, compared with unaffected control animals (Table 2). Similarly, pancreatic tissue exhibited normal ducts and normal endocrine and exocrine structures in both mutant and control animals (data not shown).

Table 2. Intrahepatic biliary profiles of 3-wk-old *wpk/wpk* rats[a]

	Wistar-*wpk/wpk*	Wistar-+/+
Portal areas/100 veins	16.6 ± 2.7	14.9 ± 2.2
Bile ductules/portal area	1.27 ± 0.13	1.19 ± 0.07

[a] The development of the biliary system is expressed as the number of recognizable portal areas, relative to the total number of vein profiles. Bile ductules/portal area is a measure of biliary proliferation. Numbers are given as means ± SD. The differences are not statistically significant.

(Wistar-+/wpk × BB-DP)F1 +/wpk Intercross

In our (Wistar-+/*wpk* × BB-DP)F1 intercross, F1 +/*wpk* hybrids were identified by progeny testing. Evaluation of aged F1 male and female rats revealed no manifestations of renal cystic disease, and F1 male and female animals bred in a robust manner.

Of the 225 F2 progeny generated to date, 55 (24.4%) exhibited recessive PKD. The number of F2 *wpk/wpk* pups is consistent with that expected for the Mendelian inheritance of a single recessive trait. Detailed histologic analysis of F2 mutants was not performed.

Genetic Mapping of wpk

To test whether *wpk* is allelic with the *Cy* locus on rat chromosome 5, we crossed test-proven Wistar-+/*wpk* and SPRD-+/*Cy* heterozygotes. None of the 35 F1 pups manifested the severe, early-onset phenotype evident for either *wpk/wpk* or *Cy/Cy* rats. As expected, 17 of the 35 pups (48.5%) expressed a phenotype consistent with that described for SPRD-+/*Cy* heterozygotes. These data exclude allelism between the *wpk* and *Cy* loci.

We then performed a whole-genome scan using interval haplotype analysis, as described by Neuhaus and Beier (23). In effect, by typing markers at the ends of each chromosome, we generated a series of 20 chromosomal intervals for the 35 affected F2 progeny of the (Wistar-+/*wpk* × BB-DP)F1 intercross.

Among the progeny of an intercross, a proportion of the F2 pups inherit chromosomes that are apparently nonrecombinant (NR), that is, the alleles of markers along these chromosomes correspond to a single parental strain (in this case, either Wistar or BB-DP). In the analysis of a recessive mutation such as *wpk*, a rapid genome scan can be performed by analyzing each chromosome for the distribution of NR intervals. The fewer NR chromosomes that correspond to the unaffected parental strain (BB-DP), the less likely it is that the loci along that chromosome are randomly distributed. Accordingly, this chromosomal interval is more likely to carry the mutation.

The distribution of chromosomal intervals is evaluated by χ^2 analysis. The maximal inferred χ^2 value is calculated for each chromosomal interval and expressed as a percentage of the maximal possible χ^2 value. Previous modeling experiments have established >75% of the maximal possible χ^2 value as the threshold for linkage (23). Therefore, this strategy provides an efficient method to identify candidate chromosomes for more detailed analyses, using standard recombinational mapping techniques.

Analysis of our data set revealed 88% of the maximal possible χ^2 value for chromosome 5 and <75% of the maximal

possible χ^2 value for all other chromosomal intervals (Table 3). These data provided presumptive evidence for linkage to chromosome 5. We typed the initial cohort of 35 affected F2 pups with a series of anonymous DNA microsatellite markers spaced at approximately 20-cM intervals along this chromosome. These pups and an additional 19 F2 pups (total of 54 pups and 108 meioses) were typed with markers within 4 cM of *D5Rat73*. These data, which are summarized in Figure 5, position *wpk* within a 11.1-cM interval centered on *D5Rat73*.

We screened 146 markers to identify the 40 informative markers required for interval haplotype analysis, indicating that the polymorphism rate between the outbred Wistar and BB-DP parental strains was only 27.5%. Similarly, for the low- and high-resolution mapping studies, we screened 16 markers to identify the six (37.5%) informative markers shown in Figure 5. This low polymorphism rate was not unexpected, given that the Wistar and BB-DP strains are phylogenetically related.

Discussion

Similarities Between the Rat wpk/wpk Phenotype and Human ARPKD

The rat *wpk* model and human ARPKD exhibit numerous similarities in their clinical phenotypes and renal histopathologic features.

The majority of human patients with ARPKD are identified either *in utero* or at birth. The most severely affected fetuses exhibit enlarged echogenic kidneys and oligohydramnios because of poor fetal renal output. At birth, these neonates often exhibit a critical degree of pulmonary hypoplasia that is incompatible with survival. Renal function, although frequently compromised, is rarely a cause of neonatal death. For infants who survive the perinatal period, systemic hypertension and progressive renal failure usually evolve (4). In addition, patients with ARPKD have defects in both urine-diluting and urine-concentrating capacities. Hyponatremia, presumably resulting from defects in free water excretion, is often observed (4).

Similarly, renal cysts in *wpk/wpk* homozygotes develop *in utero*, and enlarged kidneys are palpable within the first few weeks of life. Disease progression is associated with continued renal enlargement, systemic hypertension, proteinuria, significant reductions in urine-concentrating capacity, progressive renal insufficiency, and death by 4 to 6 wk of age. As in human patients with ARPKD (30), early renal cysts in *wpk/wpk* homozygotes develop in both proximal and distal nephron segments. With disease progression, the cystic lesions in both the rat model and human ARPKD predominantly involve the cortical and medullary collecting ducts.

Although Wistar-*wpk/wpk* mutants do not express a biliary phenotype, we suspect that *wpk*-related disease expression may be modulated by the genetic background, as has been demonstrated for the *cpk* mouse model (31). Genetic backgrounds

Table 3. Haplotype analysis[a]

Chromosome	Markers	*n*	Single-Point Analysis, χ^2	Haplotype Analysis			
				Max P χ^2	exp M χ^2	% max χ^2	NR Haplotypes
1	*D1Rat8–D1Rat84*	35	4.8–0.5	70	14.6	20	19
2	*D2Rat1–D2Rat103*	35	3.9–0.5	70	27.6	39	13
3	*D3Rat3–D3Rat7*	35	2.3–6.9	70	44.8	64	7
4	*D4Rat149–D4Rat67*	34	0.3–1.2	68	28.4	41	12
5	*D5Rat125–D5Rat41*	34	66–1.4	68	60.2	88	2
6	*D6Rat105–D6Rat1*	34	3.8–2.2	68	28.4	41	12
7	*D7mit20–D7Rat115*	32	1.5–2.1	64	30.2	47	10
8	*D8Rat56–D8Rat12*	35	4.7–2.8	68	46.1	67	6
9	*D9Rat43–D9Rat1*	35	2.8–0	70	22.8	32	15
10	*D10Rat2–D10Rat47*	35	2.8–0	70	22.8	32	15
11	*D11Rat52–D11Rat37*	29	7.6–11.6	58	39.7	68	5
12	*D12Rat2–D12Rat22*	34	3.3–0.7	68	23.5	34	14
13	*D13Rat4–D13Rat157*	35	4.8–8	70	30.2	43	12
14	*D14Rat5–D14Rat51*	35	1.4–2.3	70	22.8	32	15
15	*D15Rat5–D15Rat29*	35	2.3–1.9	70	22.8	32	15
16	*D16Rat16–D16Rat21*	35	8.3–1.6	70	35.7	51	10
17	*D17Rat6–D17Rat51*	35	1.6–0.2	70	38.6	55	9
18	*D18Rat29–D18Rat13*	35	1.6–1.2	70	30.2	43	12
19	*D19Rat28–D19Rat2*	34	4.7–1.4	68	46.1	67	6
20	*D20Rat21–D20Rat29*	35	1.6–3.5	70	20.6	29	16

[a] A complete genome scan was performed with 20 chromosomal intervals flanked by proximal and distal markers, e.g., *D1Rat8* and *D1Rat84*, respectively. *n*, number of animals in the data set. χ^2 values for each marker are indicated. Max P χ^2, maximal possible χ^2 for the indicated number of animals; exp M χ^2, maximal inferred experimental χ^2; % max χ^2, percentage of the maximal possible χ^2; NR haplotypes, number of nonrecombinant haplotypes inherited from the unaffected parental strain.

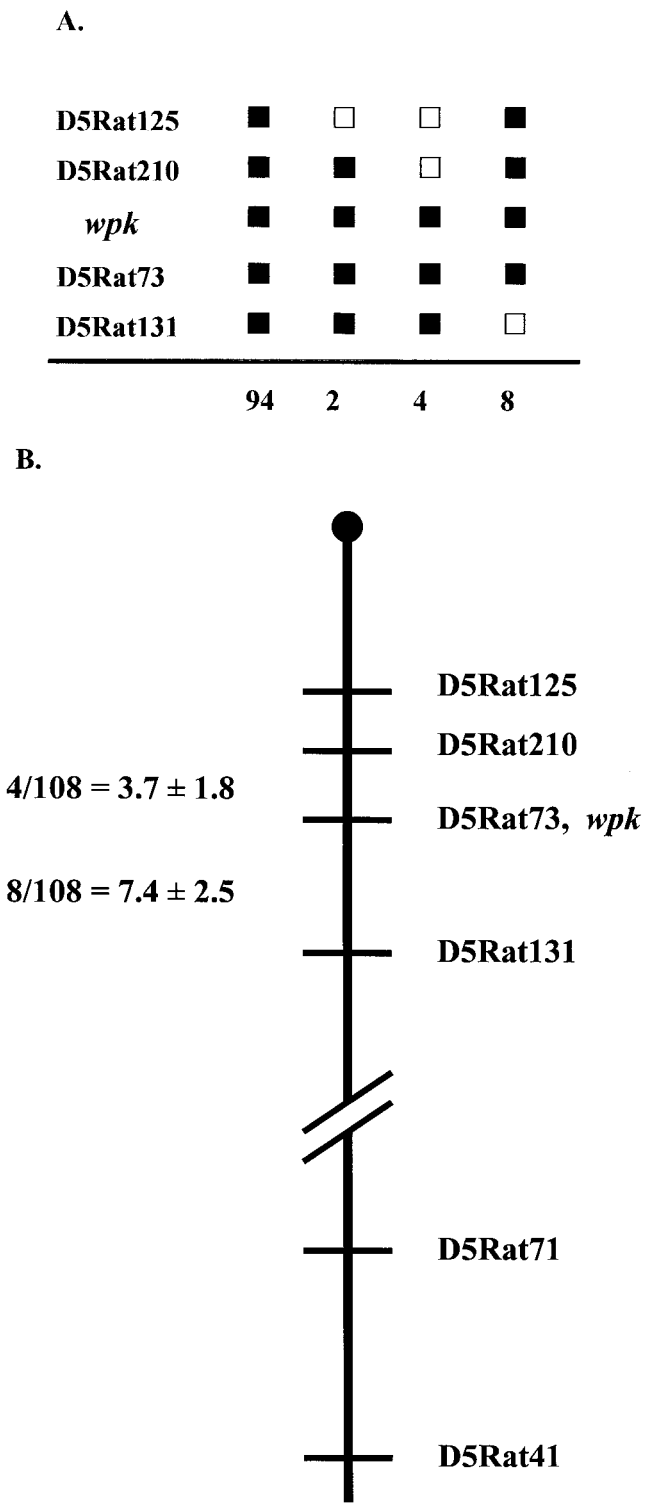

Figure 5. Genetic localization of the *wpk* locus on chromosome 5. (A) Haplotype distribution among 108 test chromosomes from the (Wistar-+/*wpk* × BB-DP)F1 intercross. For each locus, black boxes represent the inheritance of Wistar-derived alleles and white boxes represent the inheritance of BB-DP-derived alleles. The number of chromosomes for each haplotype is shown below the columns. (B) Interval between markers *D5Rat125* and *D5Rat41*, which were used in the initial interval haplotype analysis. The map distances, in centimorgans, were calculated from the recombination frequencies observed for each interval and are expressed with the standard errors.

(32–35) as well as environmental factors, such as dietary protein restriction, use of soy proteins instead of casein proteins, use of dietary flaxseeds, use of nonacidified drinking water, and potassium citrate treatment, have been reported to alter disease progression in murine PKD models (36–39). Moreover, adequate treatment of high BP may have an additional beneficial effect on both renal and patient survival rates, as it does for human patients (40).

This *wpk* model complements two established rat models of PKD, *i.e.*, the *Cy* model and the *chi* model. In contrast to both human ARPKD and the *wpk* model, the *Cy* mutation can be expressed as both a dominant and a recessive trait (14). We demonstrated that the renal phenotype in *Cy/Cy* rats is more severe than that currently described for the *wpk* model (Table 1). Histologic studies of the cysts in both *Cy/Cy* and +/*Cy* rats indicated that these may arise in any nephron segment. This is consistent with the pattern observed for human patients with ADPKD and is in contrast to the collecting tubular localization of the cysts in advanced stages of both human ARPKD and *wpk/wpk* disease. Although the *chi* model has not been as well characterized as either the *Cy* model or the *wpk* model, the *chi* model exhibits less progressive disease and includes skeletal abnormalities in addition to the renal lesions (15). In the original reports, there was no specific mention of whether biliary lesions are manifested in that model.

Systemic Hypertension

Hypertension is a common finding among human patients with PKD and contributes to both morbidity and death. Longitudinal observations indicate that hypertension is a major determinant of disease progression in ADPKD (41). Among affected children, hypertension occurs in both ADPKD and ARPKD but tends to be more severe in ARPKD (42–46).

Stimulation of the renal-angiotensin-aldosterone axis (RAAS) seems to be a major mechanism causing hypertension in ADPKD (41). Whether and to what degree increased activity of the RAAS contributes to hypertension in ARPKD remains unclear. The limited available data are conflicting. Histopathologic observations indicate that, with progressive disease, the glomeruli are compressed in the septa between expanding collecting duct cysts. Mechanical compression of the glomeruli and the intrarenal vasculature could, at least theoretically, stimulate RAAS activity. However, clinical data from affected neonates indicate that ARPKD is actually a low-renin state, with expansion of total body volume and occasional hyponatremia (40).

Given the extensive body of work on BP regulation in rats and the striking phenotypic similarities between the rat *wpk* model and human ARPKD, we propose that *wpk* rats may provide a new powerful model system for investigation of the physiologic and genetic mechanisms that contribute to hypertension in recessive PKD.

Absence of Biliary Abnormalities

In this study, we observed no biliary histopathologic features in Wistar-*wpk/wpk* homozygotes. This is a shortcoming of the model, because bile duct proliferation and periportal fibrosis

are typically present in all patients with ARPKD. However, because we did not examine the liver histologic features of F2 *wpk/wpk* homozygotes, we cannot exclude the possibility that the genetic background affects the expression of biliary lesions in the *wpk* model, as has been demonstrated for the *cpk* mouse model of ARPKD (31,47).

Cellular Morphologic Features of wpk/wpk Renal Cysts

Characterization of the cystic epithelia in the *wpk* model has yielded a number of interesting insights. First, the initial cysts seem to be derived from functioning unobstructed nephrons, and the cystic epithelia maintain their segment-specific phenotypes. These observations are consistent with data for the mouse *bpk* and *cpk* models and suggest that the disease-susceptibility genes in these models do not disrupt the early stages of nephrogenesis, *i.e.*, induction of mesenchyme-to-epithelium transformation, acquisition of stem cell character, fate determination, epitheliogenesis, and polarization (48).

In more advanced disease, cysts in the Wistar-*wpk/wpk* kidneys are lined by well differentiated collecting duct cells, as assessed by segment-specific marker profiling and EM. Although the cystic epithelia seem to have escaped the normal mechanisms controlling tubular diameter, they retain specific epithelial phenotypes, with heterogeneous populations of principal cells and intercalated cells, and maintain their organization as monolayers. Interestingly, the cyst epithelium is not uniformly proliferative, with focal areas of increased proliferation adjacent to cysts. This observation suggests that cell proliferation is influenced by local environmental factors as well as by the defective gene. Interestingly, no abnormalities of the extracellular matrix or the basal lamina were associated with renal cyst initiation or progression in *wpk/wpk* kidneys.

The wpk Mutation as a New Model of Recessive PKD

The renal phenotype of the rat *wpk* model closely resembles those of human ARPKD and the mouse *cpk*, *bpk*, and *orpk* models. However, the *wpk* model is genetically distinct from all previously described PKD loci. The *wpk* locus maps to proximal chromosome 5. Although the rat *Cy* locus also maps to chromosome 5 (49), we have demonstrated that *wpk* and *Cy* are not allelic.

In homology mapping, the human *wpk* ortholog maps to chromosome 8q11 (http://www.ncbi.nlm.nih.gov/Homology). These data exclude the *wpk* locus as a candidate for the human ARPKD gene, *PKHD1*, which maps to human chromosome 6p21-p12 (50). Similarly, the mouse *wpk* ortholog maps to proximal mouse chromosome 4 and thus is genetically distinct from mouse *bpk* on chromosome 10 (25), *cpk* on chromosome 12 (51), and *orpk* on chromosome 14 (52). It is interesting to note, however, that a principal modifying gene for both the mouse *cpk* and *pcy* models also maps to proximal chromosome 4 (35,53). This observation raises the interesting possibility that the mouse *wpk* ortholog may be a candidate PKD-modifying gene.

Although the (Wistar-+/*wpk* × BB-DP)F1 intercross was informative for localizing the rat *wpk* gene, the fact that the mutation arose in an outbred strain, coupled with the low polymorphism rate for the two parental strains, presents problems for further refinement of the genetic interval and application of positional cloning strategies to identify the *wpk* gene. Therefore, we are currently generating a congenic Wistar-+/*wpk* strain using a standard backcross strategy. By the 10th backcross generation, >99% of the genome in this congenic line will be derived from the inbred Wistar strain. At that point, we will generate a new F2 cohort by breeding the congenic Wistar-+/*wpk* line with a second inbred strain, *e.g.*, Brown Norway, so that the polymorphism rate for the two parental strains is more robust. We will also monitor the available databases for potential candidate genes that map to the candidate *wpk* region on rat chromosome 5 or the homologous regions in the human and/or mouse genomes.

Conclusions

We have characterized the clinical and histopathologic phenotypes of a new rat PKD model. Like the mouse *cpk* and *bpk* models, the rat *wpk* model strongly resembles human ARPKD. However, the hepatobiliary lesions typically associated with human disease were not observed in affected *wpk/wpk* rats. Homology mapping indicated that the rat *wpk* gene is distinct from the human ARPKD gene, *PKHD1*, as well as from the rat *Cy* gene and the mouse *cpk* and *bpk* genes. Because the Wistar-*chi* locus has not been mapped, complementation testing would be required to determine whether the *chi* and *wpk* mutations are allelic. In addition to the identification of a new gene involved in the pathogenesis of recessive PKD, this new rat mutation provides an excellent experimental model for study of the renal pathophysiologic processes associated with recessive PKD.

Acknowledgments

We thank D. R. Beier, M.D., Ph.D., for helpful discussions and C. E. Klein, R. N. Brigoos, and J. Mahabier for tender animal care. Preliminary reports of these findings were presented at the annual meetings of the American Society of Nephrology in 1997 and 1999 and have appeared in abstract form. The locus symbol, *wpk*, has been submitted to RATMAP (the rat genome database) for approval and reservation. These studies were supported by the Dutch Kidney Foundation (Dr. Nauta) and the National Institutes of Health (Grant DK51034 to Dr. Guay-Woodford).

References

1. Fick G, Gabow P: Hereditary and acquired cystic disease of the kidney. *Kidney Int* 46: 951–964, 1994
2. Gabow P, Grantham J: Polycystic kidney disease. In: *Diseases of the Kidney*, edited by Schrier R, Gottschalk C, Boston, Little, Brown, 1997, pp 521–560
3. Antignac C, Kleinknecht C, Habib R: Toward identification of a gene for familial nephronophthisis (autosomal recessive medullary cystic kidney disease). *Adv Nephrol* 24: 379–393, 1995
4. Guay-Woodford LM: Autosomal recessive disease: Clinical and genetic profiles. In: *Polycystic Kidney Disease*, edited by Watson ML, Torres VE, Oxford, UK, Oxford University Press, 1996, pp 237–267
5. European Polycystic Kidney Disease Consortium: The polycystic kidney disease 1 gene encodes a 14 kb transcript and lies

within a duplicated region on chromosome 16. *Cell* 77: 881–894, 1994
6. Mochizuki T, Wu G, Hayashi T, Xenophontos SL, Veldhuizen B, Saris JJ, Reynolds DM, Cai Y, Gabow PA, Pierides A, Kimberling WJ, Breuning MH, Deltas CC, Peters DJ, Somlo S: PKD2, a gene for polycystic kidney disease that encodes an integral membrane protein. *Science (Washington DC)* 272: 1339–1342, 1996
7. Zerres K, Mucher G, Bachner L, Deschennes G, Eggermann T, Kaariainen H, Knapp M, Lennert T, Misselwitz J, von Muhlendahl K, Neuman HPH, Pirson Y, Rutnick-Schöneborn S, Steinbicker V, Wirth B, Schärer K: Mapping of the gene for autosomal recessive polycystic kidney disease (ARPKD) to chromosome 6p21-cen. *Nat Genet* 7: 429–432, 1994
8. Guay-Woodford LM, Muecher G, Hopkins SD, Avner ED, Germino GG, Guillot AP, Herrin J, Holleman R, Irons DA, Primack W, Thomson PD, Waldo FB, Lunk PW, Zerres K: The severe perinatal form of autosomal recessive polycystic kidney disease (ARPKD) maps to chromosome 6p21.1-p12: Implications for genetic counseling. *Am J Hum Genet* 56: 1101–1107, 1995
9. Qian F, Watnick T, Onuchic L, Germino G: The molecular basis of focal cyst formation in human autosomal dominant polycystic kidney disease type I. *Cell* 87: 979–987, 1996
10. Wu G, D'Agati V, Cai Y, Markowitz G, Park JH, Reynolds DM, Maeda Y, Le TC, Hou H Jr, Kucherlapati R, Edelmann W, Somlo S: Somatic inactivation of Pkd2 results in polycystic kidney disease. *Cell* 93: 177–188, 1998
11. McDonald RA, Avner ED: Mouse models of polycystic kidney disease. In: *Polycystic Kidney Disease*, edited by Watson ML, Torres VE, Oxford, UK, Oxford University Press, 1996, pp 63–87
12. Cowley BD, Gattone VH: *In vivo* models of PKD in non-murine species. In: *Polycystic Kidney Disease*, edited by Watson ML, Torres VE, Oxford, UK, Oxford University Press, 1996, pp 88–110
13. Schieren G, Pey R, Bach J, Hafner M, Gretz N: Murine models of polycystic kidney disease. *Nephrol Dial Transplant* 11[Suppl 6]: 38–45, 1996
14. Gretz N, Kranzlin B, Pey R, Schieren G, Bach J, Obermuller N, Ceccherini I, Kloting I, Rohmeiss P, Bachmann S, Hafner M: Rat models of autosomal dominant polycystic kidney disease. *Nephrol Dial Transplant* 11[Suppl 6]: 46–51, 1996
15. Ohno K, Kondo K: A mutant rat with congenital skeletal abnormalities and polycystic kidneys. *Exp Anim* 38: 139–146, 1989
16. Schäfer K, Gretz N, Bader M, Oberbaumer I, Eckardt K, Kriz W, Bachmann S: Characterization of the Han:SPRD rat model for hereditary polycystic kidney disease. *Kidney Int* 46: 134–152, 1994
17. Nauta J, Goedbloed MA, Luider TM, Hoogeveen ATH, van den Ouwenland AMW, Halley DJJ: The Han:SPRD rat is not a genetic model of human autosomal dominant polycystic kidney disease. *Lab Anim* 31: 241–247, 1997
18. van Dokkum RPE, Jacob HJ, Provoost AP: Genetic differences define severity of renal damage after L-NAME-induced hypertension. *J Am Soc Nephrol* 9: 363–371, 1998
19. Nauta J, Ozawa Y, Sweeney W, Rutledge J, Avner E: Renal and biliary abnormalities in a new murine model of autosomal recessive polycystic kidney disease. *Pediatr Nephrol* 7: 163–172, 1993
20. van Leer EHG, de Roo GM, Bruijn JA, Hoedemaeker PJ, de Heer E: Synergistic effects of anti-gp330 and anti-dipeptidyl peptidase type IV antibodies in the induction of glomerular damage. *Exp Nephrol* 48: 1–13, 1993
21. Demarchez M, Hatmann DJ, Herbage D, Ville G, Prunieras M: Wound healing of human skin transplanted onto the nude mouse: An immunohistological and ultrastructural study of the epidermal basement membrane zone reconstruction and connective tissue reorganization. *Dev Biol* 121: 119–129, 1987
22. Havenith MG, Dingemans KP, Cleutjens JPM, Wagenaar SS, Bosman FT: Basement membranes in bronchogenic squamous cell carcinoma: An immunohistochemical and ultrastructural study. *Ultrastruct Pathol* 14: 51–63, 1990
23. Neuhaus I, Beier D: Efficient localization of mutations by interval haplotype analysis. *Mamm Genome* 9: 150–154, 1998
24. Szpirer C, Szpirer J, Van Vooren P, Tissir F, Simon JS, Koike G, Jacob HJ, Lander ES, Helou K, Kinga-Levan K, Levan G: Gene-based anchoring of the rat genetic linkage and cytogenetic maps: New regional localizations, orientation of the linkage groups, and insights into mammalian chromosome evolution. *Mamm Genome* 9: 721–734, 1998
25. Guay-Woodford L, Bryda E, Christine B, Lindsey J, Collier W, Avner E, D'Eustachio P, Flaherty L: Evidence that two phenotypically distinct mouse PKD mutations, *bpk* and *jcpk*, are allelic. *Kidney Int* 50: 1158–1165, 1996
26. Welling LW, Grantham JJ: Cystic diseases of the kidney. In: *Renal Pathology*, edited by Tisher CC, Brenner BM, Philadelphia, Lippincott, 1989, pp 1233–1277
27. Trudel M, Barisoni L, Lanoix J, D'Agati V: Polycystic kidney disease in SBM transgenic mice: Role of c-myc in disease induction and progression. *Am J Pathol* 152: 219–229, 1998
28. Verlander VJ, Madsen KM, Tisher CC: Effect of acute respiratory acidosis on two populations of intercalated cells in the rat cortical collecting duct. *Am J Physiol* 253: F1142–F1156, 1987
29. Venkatachalam MA, Kriz W: Anatomy. In: *Heptinstall's Pathology of the Kidney*, 5th Ed., edited by Jennette JC, Olson JL, Schwartz MM, Silva FG, Philadelphia, Lippincott, 1998, pp 3–66
30. Sweeney W, Avner E: Proximal tubular cysts in fetal human ARPKD [Abstract]. *J Am Soc Nephrol* 9: 1953A, 1998
31. Guay-Woodford LM, Green WJ, Lindsey JR, Beier DR: Germline and somatic loss-of-function of the mouse cpk gene causes biliary ductal pathology that is genetically modulated. *Hum Mol Genet* 9: 769–778, 2000
32. Iakoubova O, Dushkin H, Beier D: Genetic analysis of a quantitative trait in a mouse model of polycystic kidney disease. *Am J Respir Crit Care Med* 156(Suppl): S72–S77, 1997
33. Guay-Woodford LM, Wright CJ, Walz G, Churchill GA: Quantitative trait loci modulate renal cystic disease severity in the mouse bpk model. *J Am Soc Nephrol* 11:1253–1260, 2000
34. Upadhya P, Churchill G, Birkenmeier E, Barker J, Frankel W: Genetic modifiers of polycystic kidney disease in intersubspecific KAT2J mutants. *Genomics* 58: 129–137, 1999
35. Woo D: Progression of polycystic kidney disease in pcy mice is a quantitative trait under polygenic control. *J Clin Invest* 100: 1934–1940, 1998
36. Cowley BD Jr, Grantham JJ, Muessel MJ, Kraybill AL, Gattone VH II: Modification of disease progression in rats with inherited polycystic kidney disease. *Am J Kidney Dis* 27: 865–879, 1996
37. Ogborn MR, Bankovic-Calic N, Shoesmith C, Buist R, Peeling J: Soy protein modification of rat polycystic kidney disease. *Am J Physiol* 274: F541–F549, 1998

38. Ogborn MR, Nitschmann E, Weiler H, Leswick D, Bankovic-Calic N: Flaxseed ameliorates interstitial nephritis in rat polycystic kidney disease. *Kidney Int* 55: 417–423, 1999
39. Tanner GA: Potassium citrate/citric acid intake improves renal function in rats with polycystic kidney disease. *J Am Soc Nephrol* 9: 1242–1248, 1998
40. Kaplan B, Fay J, Shah V: Autosomal recessive polycystic kidney disease. *Pediatr Nephrol* 3: 43–49, 1989
41. Chapman A, Gabow P: Hypertension in autosomal dominant polycystic kidney disease. *Kidney Int* 52[Suppl 61]: S71–S73, 1997
42. Zerres K, Rudnik-Schoneborn S, Deget T, Holtkamp U, Brodehl J, Geisert J, Scharer K: Autosomal recessive polycystic kidney disease in 115 children: Clinical presentation, course and influence of gender: Arbeitsgemeinschaft fur Padiatrische, Nephrologie. *Acta Paediatr* 85: 437–445, 1996
43. Kääriääinen H, Koskiemis O, Norio R: Dominant and recessive polycystic kidney disease in children: Evaluation of clinical features and laboratory data. *Pediatr Nephrol* 2: 296–302, 1988
44. Roy S, Dillon MJ, Trompeter RS, Barratt TM: Autosomal recessive polycystic kidney disease: Long-term outcome of neonatal survivors. *Pediatr Nephrol* 11: 302–306, 1997
45. Gabow PA, Johnson AM, Kaehny WD, Kimberling WJ, Lezotte DC, Duley ET, Jones RH: Factors affecting the progression of renal disease in autosomal dominant polycystic kidney disease. *Kidney Int* 41: 1311–1319, 1992
46. Watson ML: Hypertension in polycystic kidney disease. In: *Oxford Textbook of Clinical Nephrology*, edited by Watson ML, Torres VE, Oxford, Oxford Press, 1996, pp 407–429
47. Gattone V, MacNaughton K, Kraybill A: Murine autosomal recessive polycystic kidney disease with multiorgan involvement induced by the cpk gene. *Anat Rec* 245: 488–499, 1996
48. Davies J: Mesenchyme to epithelial transition during development of the mammalian kidney tubule. *Acta Anat* 156: 187–201, 1996
49. Bihoreau M, Ceccherini I, Browne J, Kranzlin B, Romeo G, Lathrop G, James M, Gretz N: Location of the first genetic locus, PKDr1, controlling autosomal dominant polycystic kidney disease in Han:SPRD *cy*/+ rat. *Hum Mol Genet* 6: 609–613, 1997
50. Mucher G, Becker J, Knapp M, Buttner R, Moser M, Rudnik-Schoneborn S, Somlo S, Germino G, Onuchic L, Avner E, Guay-Woodford L, Zerres K: Fine mapping of the autosomal recessive polycystic kidney disease locus (PKHD1) and the genes MUT, RDS, CSNK2 beta, and GSTA1 at 6p21.1-p12. *Genomics* 48: 40–45, 1998
51. Simon E, Cook S, Davisson M, D'Eustachio P, Guay-Woodford L: The mouse congenital polycystic kidney (cpk) locus maps within 1.3 cM of the chromosome 12 marker D12Nyu2. *Genomics* 21: 415–418, 1994
52. Onuchic L, Schrick J, Ma J, Hudson T, Guay-Woodford L, Zerres K, Woychik R, Reeders S: Sequence analysis of the human hTg737 gene and its polymorphic sites in patients with autosomal recessive polycystic kidney disease. *Mamm Genome* 6: 805–808, 1995
53. Woo D, Miao S, Tran T: Progression of polycystic kidney disease in cpk mice is a quantitative trait under polygenic control [Abstract]. *J Am Soc Nephrol* 6: 731A, 1995